

Computational Science Laboratory Report
CSL-TR-2024-2
March 21, 2024

Abhinab Bhattacharjee, Andrey A. Popov,
Arash Sarshar, Adrian Sandu

*“Improving the Adaptive Moment Estimation
(ADAM) stochastic optimizer through an
Implicit-Explicit (IMEX) time-stepping
approach”*

Computational Science Laboratory
“Compute the Future!”

Department of Computer Science
Virginia Tech
Blacksburg, VA 24060
Phone: (540) 231-2193
Fax: (540) 231-6075
Email: abhinab93@vt.edu
Web: <https://cs1.cs.vt.edu>



Improving the Adaptive Moment Estimation (ADAM) stochastic optimizer through an Implicit-Explicit (IMEX) time-stepping approach

Abhinab Bhattacharjee^{*1}, Andrey A. Popov^{†1,2}, Arash Sarshar^{‡3} and Adrian Sandu^{§1}

¹Computational Science Lab, Department of Computer Science, Virginia Tech

²The Oden Institute for Computational Engineering and Sciences, The University of Texas at Austin

³California State University, Long Beach

Abstract

The ADAM optimizer, often used in Machine Learning for neural network training, corresponds to an underlying ordinary differential equation (ODE) in the limit of very small learning rates. This work shows that the classical ADAM algorithm is a first order implicit-explicit (IMEX) Euler discretization of the underlying ODE. Employing the time discretization point of view, we propose new extensions of the ADAM scheme obtained by using higher order IMEX methods to solve the ODE. Based on this approach, we derive a new optimization algorithm for neural network training that performs better than classical ADAM on several regression and classification problems.

*abhinab93@vt.edu

†andrey.a.popov@utexas.edu

‡arash.sarshar@csulb.edu

§asandu7@vt.edu

1 Introduction

Neural network (NN) training requires to solve unconstrained optimization problems [3] of the form

$$\theta^* = \arg \min_{\theta} \mathcal{L}([X, Y], \widehat{Y}; \theta) \quad \text{subject to} \quad \widehat{Y} = f(X, \theta), \quad (1)$$

where $[X, Y]$ are the input-output pairs of the training data set, f is some parameterized NN (with θ as parameters), θ^* are the optimal parameters, \mathcal{L} is some loss function, and \widehat{Y} is the output of the NN for the input X .

Stochastic Gradient Descent (SGD), inspired from the early work [6], trains NNs using subsets (batches) of data to manage large datasets. It is employed in many deep learning applications such as regression, image classification, or sequence modeling [14, 17, 18]. However, it often suffers from unwanted oscillations when small batches are used. Momentum methods [22, 23] extend gradient descent by keeping track of the direction of persistent decrease of loss function, which helps reduce oscillations introduced by stochastic behavior.

First order adaptive optimization methods use the past history of gradient evaluations to improve convergence. The adaptivity stems from the change in the learning rate according to the exponential moving average of past gradients. Some of the well known adaptive methods are ADAGRAD [10], RMSPROP [34], ADADELTA [36], ADAM [16] and others [35]. This study focuses on ADAM, one of the most successful and widely used optimizers in deep learning [4, 19, 24]. The algorithm is summarized in Appendix A.

It was shown in [9] that, in the limit of small learning rates, adaptive methods approach a continuous dynamical system called “the underlying ODE” [24]. Similarly, in the limit, batch training leads to underlying stochastic differential equations. Taking advantage of the continuous formulation of the optimization problem, we propose the use of high order schemes to discretize the underlying ODE, and derive new discrete optimization algorithms for NN training. Discretization of stochastic differential equations, leading to new stochastic training algorithms, is not studied in this paper and will be addressed in future work.

The novel contributions of this work are as follows:

- We interpret ADAM as first order Generalized Additive Runge-Kutta (GARK) [26] IMEX Euler discretization of the underlying ODE. This formulation recovers the original algorithm proposed in [16].
- We propose a second order Trapezoidal IMEX method for the discretization of the underlying ODE. Numerical experiments show that the resulting discrete algorithm performs similar or better than standard ADAM in a number of regression and classification problems.

The remainder of this paper is organized as follows. Section 2 provides the background and motivation for this study. Section 3 introduces the formulation of ADAM as a numerical discretization of the underlying ODE. Employing high order discretization techniques allows to develop new optimization algorithms. Section 4 reports numerical experiment results. Section 5 concludes the study with a summary of the best method we found, and discusses several future extensions.

2 Background

This work focuses on the ADAM numerical optimization procedure used for training deep feedforward and convolutional networks.

2.1 Performance of Optimization for NN Training

The ADAM algorithm [16] is summarized in Algorithm 2. It has several tunable parameters such as β -s (determine the amount of information that is carried from one epoch to the next, or equivalently, how much is exponentially lost/forgotten from the last step/epoch with or without batching) and the learning rate (h). ADAM is an “adaptive” learning algorithm because it scales the learning rate by the velocity (h/\sqrt{v}).

ADAM can be rewritten (in discrete setting) as follows:

$$\begin{aligned}
 g_{n+1} &= \nabla_{\theta} \mathcal{L}(t_{n+1}, \theta_n) , \\
 m_{n+1} &= (1 - \beta_1) \sum_{i=0}^{n+1} \beta_1^i g_{n+1-i} , \\
 v_{n+1} &= (1 - \beta_2) \sum_{i=0}^{n+1} \beta_2^i g_{n+1-i}^{\circ 2} , \\
 \theta_{n+1} &= \theta_n - h \frac{(1 - \beta_1) \sum_{i=0}^{n+1} \beta_1^i g_{n+1-i}}{\sqrt[{\circ}]{(1 - \beta_2) \sum_{i=0}^{n+1} \beta_2^i g_{n+1-i}^{\circ 2}}} ,
 \end{aligned} \tag{2}$$

where the following short hand notation is used:

$$\mathcal{L}(t_{n+1}, \theta) := \nabla_{\theta} \mathcal{L}([X, Y]_{n+1}, \widehat{Y}_{n+1}; \theta),$$

where $t_{n+1} = t_n + h$. The hyper-parameters β (consequently the α ’s used in [9]) should be tuned according to the loss function which depends on the problem. It is known that the original β values perform worse than SGD in a contrived problem [9, 24].

It has been shown that the discrete-time ADAM algorithm in eq. (2), in the limit of small learning rates as $h \rightarrow 0$, has a continuous-time counterpart in the form of an ordinary differential equation [9]:

$$\begin{aligned}
 \dot{\theta}(t) &= -m(t) / \sqrt[{\circ}]{v(t)} + \epsilon, \\
 \dot{m}(t) &= d(t) \nabla_{\theta} \mathcal{L}(t, \theta(t)) - r(t) m(t), \\
 \dot{v}(t) &= p(t) [\nabla_{\theta} \mathcal{L}(t, \theta(t))]^{\circ 2} - q(t) v(t),
 \end{aligned} \tag{3}$$

where $[\cdot]^{\circ 2}$ is used for element-wise square operation, $\sqrt[{\circ}]{\cdot}$ for element-wise square root, $[\cdot]/[\cdot]$ for element-wise division, and “ t ” denotes the time component in the continuous setting. We use the short hand notation

$$\mathcal{L}(t, \theta) := \mathcal{L}([X_t, Y_t], \widehat{Y}_t; \theta), \tag{4}$$

where X_t, Y_t represent the input and output data at time t , and \widehat{Y}_t is the model outputs at time t .

The ϵ in the denominator of first equation is added for numerical stability and is fixed in this study ($\epsilon = 1e-8$), though there is evidence to suggest that ϵ plays a role in the converge of the algorithm [7]. The values of the time dependent parameters $d(t), r(t), p(t)$ and $q(t)$ for different first order adaptive methods are given in [9]. For ADAM, the parameters are as follows:

$$\begin{aligned} d(t) = r(t) &= \frac{1}{\alpha_1}, & p(t) = q(t) &= \frac{1}{\alpha_2}, \\ \alpha_i &:= -h/\log \beta_i & \Leftrightarrow & \beta_i = e^{\frac{-h}{\alpha_i}}, \quad i = 1, 2, \end{aligned} \quad (5)$$

and depend on the learning rate h .

2.2 Optimization in the Continuous and Discrete Setting

Solving the optimization problem in continuous formulation eq. (3) comes down to solving numerically a system of ordinary differential equations. Theory about the solution of ODEs [5, 12, 13], is relevant to, but outside the scope of this study. We focus our effort on ODEs of the form:

$$\dot{y} = f(t, y), \quad t \in [t_0, t_f], \quad y(t_0) = y_0, \quad (6)$$

where f represents the non-linear dynamics, y_0 represents the initial conditions, and t_0 to t_f represents the timespan of interest.

Two simple numerical methods for solving eq. (6) are the explicit Forward Euler (FE) scheme

$$y_{n+1} = y_n + h f(t_n, y_n), \quad (7a)$$

and the implicit Backward Euler (BE) scheme

$$y_{n+1} = y_n + h f(t_{n+1}, y_{n+1}). \quad (7b)$$

Explicit methods like eq. (7a) are computationally inexpensive per step. In contrast, implicit methods like eq. (7b) require the solution of a (non-)linear system of equations to compute y_{n+1} , and are therefore computationally expensive per step. Implicit schemes deliver a computational benefit when the ODE is stiff [8]: Due to stability limits, the solution of a stiff equation within a desired accuracy requires a significantly smaller time step for an explicit method when compared to an implicit one [1, 12, 13]. Combining the best of both worlds, IMEX methods were developed, where we split the right-hand side of the ODE into a stiff and a non-stiff part; an implicit scheme is used for the stiff part and an explicit scheme for the non-stiff part. This idea is the core of this study and is explained in more detail in section 3.1.

Following [9], the FE discretization of the optimization ODE eq. (3) is:

$$\begin{aligned} \theta_{n+1} &= \theta_n - h m_n / \sqrt[3]{v_n + \epsilon}, \\ m_{n+1} &= m_n [1 - h r(t_n)] + h d(t_n) \nabla_{\theta} \mathcal{L}(t_n, \theta_n), \\ v_{n+1} &= v_n [1 - h q(t_n)] + h p(t_n) [\nabla_{\theta} \mathcal{L}(t_n, \theta_n)]^{\circ 2}. \end{aligned} \quad (8)$$

The discretization time step h is also known as the “learning rate” in ML literature, and the two terms will often be used interchangeably in this study. Subscripts n represent the algorithmic discrete time (often called “epoch” in ML literature). This notation holds true for training in small batches of data, albeit with a minor change (refer to the remark in section 2.2) Note the similarities and differences between the formulation in eq. (8) and the one given in Algorithm 2. More accurate algorithms for solving the ODE eq. (6) are offered by the class of Runge-Kutta (RK) methods [12].

Remark. *When there is no batching in training, the ODE eq. (3) is continuous across all time steps(epochs.) However, using a batch of data to calculate an approximate gradient in the time interval $t_n \leq t \leq t_{n+1}$ can lead to a point-wise discontinuity at the start and end of the intervals. From a practical implementation point of view, this is not an issue for us, as can be seen in section 4.*

The following assumptions are considered:

Assumptions. *The loss function is defined as $\mathcal{L}([X, Y], \hat{Y}; \theta) : \mathbb{R}^{p \times d} \rightarrow \mathbb{R}$, where p and d are the dimensions of the parameter and input space. Loss is considered to be C^2 continuous over the parameter space. The gradient of the loss is also considered Lipschitz continuous such that*

$$\exists C > 0, \left\| \nabla_{\theta} \mathcal{L}([X, Y], \hat{Y}; \theta_m) - \nabla_{\theta} \mathcal{L}([X, Y], \hat{Y}; \theta_n) \right\| \leq C \|\theta_m - \theta_n\| \quad \forall (\theta_m, \theta_n) \in \mathbb{R}^p$$

and $([X, Y], \hat{Y})$ are the input, output data, and the predicted neural network output, respectively. This Lipschitz continuity is useful when considering noisy data, such as the case of batching, and guarantees the boundedness of the gradient. Since the gradient also appears on the right-hand side of the ODE system eq. (6), this assumption is also necessary for the existence of the numerical solution of eq. (6).

Remark. *The β s from the original ADAM [16] and the α s from the ODE formulation of the adaptive methods [9] are related through the relation given by eq. (5). It is important to note that the α ’s need to be calculated from the β ’s using the given relationship and vice-versa.*

3 Proposed Methodology

3.1 IMEX GARK Time Integration

We consider now the case of ODEs eq. (6) that can be naturally split into a non-stiff part and a stiff part:

$$\begin{bmatrix} \dot{y} \\ \dot{z} \end{bmatrix} = \begin{bmatrix} f(t, y, z) \\ g(t, y, z) \end{bmatrix}, \quad \begin{bmatrix} y(t_0) \\ z(t_0) \end{bmatrix} = \begin{bmatrix} y_0 \\ z_0 \end{bmatrix}, \quad (9)$$

where y are the non-stiff components with $f(\cdot)$ the non-stiff dynamics, and z are the stiff components with $g(\cdot)$ the stiff dynamics of the system. Solving the entire system eq. (9) with an explicit method such as FE in eq. (7a) typically requires unacceptably small step sizes due to the stability restrictions imposed by the stiff part [12, 13]. Conversely, solving the entire system eq. (9) with an implicit method like BE eq. (7b) results in large nonlinear

systems of equations that couple all the variables, both stiff and non-stiff, whose solution is computationally expensive and often intractable in higher dimensional systems.

An intuitive idea is to solve the non-stiff part with an inexpensive explicit scheme and the stiff part with a stable implicit method. Taking advantage of both methods gave rise to the class of Implicit-Explicit (IMEX) [2] time discretization methods. For example, one can solve eq. (9) as follows: First, advance the non-stiff component from y_n at time t_n to y_{n+1} at time t_{n+1} using the FE scheme given in eq. (7a). Next, advance the stiff component from z_n at time t_n to z_{n+1} at time t_{n+1} using the BE scheme in eq. (7b). The resulting IMEX Euler method reads:

$$\begin{bmatrix} y_{n+1} \\ z_{n+1} \end{bmatrix} = \begin{bmatrix} y_n + h f(t_n, y_n, z_n) \\ z_n + h g(t_{n+1}, y_{n+1}, z_{n+1}) \end{bmatrix}. \quad (10)$$

Note that in eq. (10) we first solve the explicit component, i.e., the first equation, and then use y_{n+1} in the solution of the second equation. As a result, The nonlinear system needs to be solved only for the stiff components z_{n+1} .

This paper focuses on applying IMEX methods to solve the optimization ODE in eq. (3). We consider Generalized-structure Additive Runge-Kutta (GARK) family of methods [26], which are a generalized formulation of earlier partitioned Runge-Kutta schemes [15].

A two-way partitioned (diagonally implicit) GARK method with stepsize h solves the component partitioned system eq. (9) as follows [26]:

$$\begin{bmatrix} Y_i^E \\ Z_i^E \end{bmatrix} = \begin{bmatrix} y_n + h \sum_{j=1}^{i-1} a_{i,j}^{E,E} f(T_j^E, Y_j^E, Z_j^E) \\ z_n + h \sum_{j=1}^{i-1} a_{i,j}^{E,I} g(T_j^I, Y_j^I, Z_j^I) \end{bmatrix}, \quad (11a)$$

$$\begin{bmatrix} Y_i^I \\ Z_i^I \end{bmatrix} = \begin{bmatrix} y_n + h \sum_{j=1}^i a_{i,j}^{I,E} f(T_j^E, Y_j^E, Z_j^E) \\ z_n + h \sum_{j=1}^i a_{i,j}^{I,I} g(T_j^I, Y_j^I, Z_j^I) \end{bmatrix}, \quad (11b)$$

$$\begin{bmatrix} y_{n+1} \\ z_{n+1} \end{bmatrix} = \begin{bmatrix} y_n + h \sum_{i=1}^{s^E} b_i^E f(T_i^E, Y_i^E, Z_i^E) \\ z_n + h \sum_{i=1}^{s^I} b_i^I g(T_i^I, Y_i^I, Z_i^I) \end{bmatrix}. \quad (11c)$$

Here $(\mathbf{A}^{E,E}, \mathbf{b}^E, \mathbf{c}^E)$ is an explicit Runge-Kutta method ($a_{i,j}^{E,E} = 0$ for $j \geq i$) used to solve the non-stiff component. Similarly, $(\mathbf{A}^{I,I}, \mathbf{b}^I, \mathbf{c}^I)$ is a diagonally implicit Runge-Kutta method ($a_{i,j}^{I,I} = 0$ for $j > i$) used to solve the stiff component. The matrices $\mathbf{A}^{E,I}$ and $\mathbf{A}^{I,E}$ realize the coupling between the non-stiff and the stiff components. The time argument is evaluated as

$$T_j^E = t_n + hc_j^E, \quad T_j^I = t_n + hc_j^I, \quad (11d)$$

This method can be summarized in the following Butcher tableau:

$$\begin{array}{c|cc} \mathbf{c}^E & \mathbf{A}^{E,E} & \mathbf{A}^{E,I} \\ \mathbf{c}^I & \mathbf{A}^{I,E} & \mathbf{A}^{I,I} \\ \hline & \mathbf{b}^{ET} & \mathbf{b}^{IT} \end{array}, \quad (11e)$$

with the coefficient matrices $\mathbf{A}^{u,v} \in \mathbb{R}^{s^u \times s^v}$, $\mathbf{b}^u \in \mathbb{R}^{s^u}$, $\mathbf{c}^u = \mathbf{A}^{u,v} \cdot \mathbf{1}^v \in \mathbb{R}^{s^u}$, and $\mathbf{1}^v \in \mathbb{R}^{s^v}$ a vector of ones, for $u, v \in \{E, I\}$. The internal consistency conditions $\mathbf{A}^{E,I} \cdot \mathbf{1}^I = \mathbf{c}^E$ and $\mathbf{A}^{I,E} \cdot \mathbf{1}^E = \mathbf{c}^I$ are assumed to be satisfied [26]. For example, the IMEX Euler method in

eq. (10) is a GARK scheme eq. (11) characterized by the following Butcher tableau eq. (11e):

$$\begin{array}{c|c|c} 0 & 0 & 0 \\ \hline 1 & 1 & 1 \\ \hline & 1 & 1 \end{array} \quad (12)$$

3.2 ADAM as the IMEX Euler Discretization

We will now demonstrate how the ADAM method fits in the GARK scheme eq. (11e). We perform a component splitting of the ADAM ODE eq. (3) as follows:

$$z = \begin{bmatrix} \theta \\ t \end{bmatrix}, \quad y = \begin{bmatrix} m \\ v \end{bmatrix},$$

and write the system eq. (3) in partitioned form eq. (9):

$$\begin{bmatrix} \dot{y} \\ \dot{z} \end{bmatrix} = \begin{bmatrix} \dot{m} \\ \dot{v} \\ \dot{\theta} \\ \dot{t} \end{bmatrix} = \begin{bmatrix} d(t) \nabla_{\theta} \mathcal{L}(t, \theta) - r(t) m(t) \\ p(t) [\nabla_{\theta} \mathcal{L}(t, \theta)]^{\circ 2} - q(t) v(t) \\ -m(t) / \sqrt[3]{v(t) + \epsilon} \\ 1 \end{bmatrix} = \begin{bmatrix} f(t, y, z) \\ g(t, y, z) \end{bmatrix}, \quad (13)$$

where we used notation given in eq. (4). Solving the partitioned system eq. (13) with the IMEX Euler method eq. (10) with a step size h gives us the discrete-time method:

$$\begin{bmatrix} m_{n+1} \\ v_{n+1} \\ \theta_{n+1} \\ t_{n+1} \end{bmatrix} = \begin{bmatrix} m_n + h d(t_{n+1}) \nabla_{\theta} \mathcal{L}(t_{n+1}, \theta_n) - h r(t_n) m_n \\ v_n + h p(t_{n+1}) [\nabla_{\theta} \mathcal{L}(t_{n+1}, \theta_n)]^{\circ 2} - h q(t_n) v_n \\ \theta_n - h m_{n+1} / \sqrt[3]{v_{n+1} + \epsilon} \\ t_n + h \end{bmatrix}. \quad (14)$$

Note that although this is an application of the IMEX Euler method, no nonlinear systems of equations are solved in eq. (14). This is due to the special structure of eq. (13), where the stiff dynamics $g(t, y, z)$ does not depend on θ , therefore θ_{n+1} is not present on the right hand side of the third equation in eq. (14), and can be computed via an explicit update.

We compare eq. (14) with the standard ADAM. Identifying the ADAM parameters (refer eq. (14) and algorithm 2) as $\beta_1 = 1 - h r_n = 1 - h d_n$, $\beta_2 = 1 - h q_n = 1 - h p_n$, we conclude that the IMEX Euler solution eq. (14) of the optimization ODE eq. (3)–eq. (13) recovers the original discrete ADAM method. In other words, *ADAM is the IMEX Euler discretization of eq. (13)*.

3.3 Improving ADAM via High Order IMEX GARK Discretizations

When initial value problems are considered, higher order time integration schemes outperform the first order Euler method. Higher order methods have smaller local and global truncation errors and require fewer steps to reach a desired level of accuracy compared to lower order methods. We make the ansatz that improved versions of the ADAM can be obtained by applying higher order IMEX GARK schemes to the partitioned

optimization ODE eq. (13). Specifically, we investigate how higher order IMEX time discretization methods lead to better stochastic optimization algorithms, i.e., result in a faster decrease of the loss function toward a local minimum.

Application of an IMEX GARK scheme eq. (11) to solve the partitioned ADAM ODE system eq. (13) leads to the following discrete optimization algorithm [26] :

$$\begin{aligned}
m_i^E &= m_n + h \sum_{j=1}^{i-1} a_{i,j}^{E,E} (d(T_j^E) \nabla_{\theta} \mathcal{L}(T_j^E, \theta_j^E) - r(T_j^E) m_j^E), \quad i = 1, \dots, s^E, \\
v_i^E &= v_n + h \sum_{j=1}^{i-1} a_{i,j}^{E,E} (p(T_j^E) \nabla_{\theta} \mathcal{L}(T_j^E, \theta_j^E)^{\circ 2} - q(T_j^E) v_j^E), \quad i = 1, \dots, s^E, \\
m_i^I &= m_n + h \sum_{j=1}^i a_{i,j}^{I,E} (d(T_j^E) \nabla_{\theta} \mathcal{L}(T_j^E, \theta_j^E) - r(T_j^E) m_j^E), \quad i = 1, \dots, s^I, \\
v_i^I &= v_n + h \sum_{j=1}^i a_{i,j}^{I,E} (p(T_j^E) \nabla_{\theta} \mathcal{L}(T_j^E, \theta_j^E)^{\circ 2} - q(T_j^E) v_j^E), \quad i = 1, \dots, s^I, \\
\theta_i^E &= \theta_n + h \sum_{j=1}^{i-1} a_{i,j}^{E,I} \frac{-m_j^I}{\sqrt{v_j^I + \varepsilon}}, \quad i = 1, \dots, s^E, \\
m_{n+1} &= m_n + h \sum_{i=1}^{s^E} b_i^E (d(T_i^E) \nabla_{\theta} \mathcal{L}(T_i^E, \theta_i^E) - r(T_i^E) m_i^E), \\
v_{n+1} &= v_n + h \sum_{i=1}^{s^E} b_i^E (p(T_i^E) \nabla_{\theta} \mathcal{L}(T_i^E, \theta_i^E)^{\circ 2} - q(T_i^E) v_i^E), \\
\theta_{n+1} &= \theta_n + h \sum_{i=1}^{s^I} b_i^I \frac{-m_i^I}{\sqrt{v_i^I + \varepsilon}}, \\
t_{n+1} &= t_n + h.
\end{aligned} \tag{15}$$

where T_j^E and T_j^I are defined in eq. (11d).

We reiterate the fact that formulation in eq. (15) does not require any implicit (algebraic) solve since the update to θ in eq. (14) does not depend on θ . This is important as we do not want to incur the extra cost of a non-linear solve during the training on large datasets.

The coefficients of an IMEX GARK scheme employed in eq. (15) need to satisfy the order conditions developed in [26]. The IMEX Euler coefficients eq. (12) applied to eq. (15) form a first order IMEX GARK, and recover the original ADAM method [16].

In this work we focus on a second order IMEX GARK method that employs the implicit trapezoidal scheme (often called Crank Nicholson) for the stiff component, and the explicit trapezoidal scheme for the non-stiff variables. This method called ‘‘IMEX Trapezoidal’’ is

Algorithm 1 IMEX Trapezoidal ADAM Optimizer

Require: h : Step-size/Learning rate

Require: $\alpha_1, \alpha_2 \in [0, 1)$: Determines past information retention rate

Require: $\mathcal{L}(t, \theta)$: Loss/Objective function to be minimized

Require: θ_0 : Initial learnable parameters in this case

$m_0 \leftarrow 0$ (Initialize first moment vector)

$v_0 \leftarrow [\nabla_{\theta} \mathcal{L}(t_0, \theta_0)]^{\circ 2}$ (Initialize second moment vector)

$n \leftarrow 0$ (Initialize time step)

while θ_t not converged **do**

$k_1^m \leftarrow \frac{1}{\alpha_1} [\nabla_{\theta} \mathcal{L}(t_{n+1}; \theta_n) - m_n]$

$k_1^v \leftarrow \frac{1}{\alpha_2} [\nabla_{\theta} \mathcal{L}^{\circ 2}(t_{n+1}; \theta_n) - v_n]$

$k_1^{\theta} \leftarrow -\frac{m_n}{\sqrt{v_n + \epsilon}}$

$k_2^m \leftarrow \frac{1}{\alpha_1} [\nabla_{\theta} \mathcal{L}(t_{n+1}; \theta_n + h k_1^{\theta}) - (m_n + h k_1^m)]$

$k_2^v \leftarrow \frac{1}{\alpha_2} [(\nabla_{\theta} \mathcal{L}(t_{n+1}; \theta_n + h k_1^{\theta}))^{\circ 2} - (v_n + h k_1^v)]$

$k_2^{\theta} \leftarrow -\frac{(m_n + 0.5 h k_1^m + 0.5 h k_2^m)}{\sqrt{v_n + 0.5 h k_1^v + 0.5 h k_2^v + \epsilon}}$

$\theta_{n+1} \leftarrow \theta_n + \frac{1}{2} k_1^{\theta} + \frac{1}{2} k_2^{\theta}$

$m_{n+1} \leftarrow m_n + \frac{1}{2} k_1^m + \frac{1}{2} k_2^m$

$v_{n+1} \leftarrow v_n + \frac{1}{2} k_1^v + \frac{1}{2} k_2^v$

$n \leftarrow n + 1$

end while

defined by the following Butcher tableau of coefficients as developed in eq. (11e):

$$\begin{array}{c|c|c}
 \mathbf{c}^E & \mathbf{A}^{E,E} & \mathbf{A}^{E,I} \\
 \mathbf{c}^I & \mathbf{A}^{I,E} & \mathbf{A}^{I,I} \\
 \hline
 & \mathbf{b}^{ET} & \mathbf{b}^{IT}
 \end{array} = \begin{array}{c|cc|cc}
 & 0 & 0 & 0 & 0 \\
 & 1 & 1 & 0 & 1 & 0 \\
 \hline
 & 0 & 0 & 0 & 0 & 0 \\
 & 1 & \frac{1}{2} & \frac{1}{2} & \frac{1}{2} & \frac{1}{2} \\
 \hline
 & \frac{1}{2} & \frac{1}{2} & \frac{1}{2} & \frac{1}{2}
 \end{array} . \tag{16}$$

Application of the IMEX Trapezoidal method eq. (16) applied to solve the ADAM partitioned ODE eq. (13) leads to the new ‘‘IMEX Trapezoidal ADAM’’ optimization scheme. The computational steps of this method are given explicitly in Algorithm 1.

This optimization scheme performs well on several classification and regression problems, as confirmed by numerical experiments reported in Section 4. The second order IMEX method achieves a good balance between performance and number of gradient evaluations for several test cases.

4 Numerical Experiments

The experiments involving regression and classification are chosen based on their relevance in several ML and scientific computing applications. A random search is performed to find

the “best” hyperparameters for each of the experiments. To ensure robust results regardless of random initialization, every experiment is run with 20 different random initial parameter values, and the average loss is reported.

Initialization is of paramount importance for efficient learning algorithms. A good initialization can help the algorithm to converge faster to a desired local minimum. On the other hand, if the initialization is bad, an algorithm might get stuck in a valley or saddle point and never converge to the local minima [21, 33]. We resort and stick with Xavier Initialization in this study for all the experiments [11].

The momentum is initialized to zeros and the velocity to the square of the initial gradient for all the problems. Our experiments focus on minimizing the cost function and not the generalization error on test data, however, they are reported in some cases. Methods such as early stopping, drop out [31] or different regularization techniques (Lasso or Ridge) can be used to mitigate over-fitting and is not in conflict with our proposed method. Mean Square Error (MSE) is used for regression and Categorical Cross Entropy loss is used for classification problems. The decrease in cost function is measured against the total number of gradient evaluations. Higher order methods have more gradient evaluations in each epoch (or time-step) and it is fair we compare them based on the total gradient evaluations. SGD, FE discretization, IMEX ADAM and IMEX Trapezoidal methods are compared for each problem. A few other higher order RK and IMEX GARK methods were tested (refer B). However, they were not consistently performing well in all experiments and further study is needed to check if they pose any real advantage for the increased number of gradient evaluations.

4.1 Lorenz ’63 Dynamics

The Lorenz ’63 model [20] is a nonlinear chaotic system represented by equations:

$$\begin{aligned}\dot{x} &= \sigma(y - x), \\ \dot{y} &= x(\rho - z) - y, \\ \dot{z} &= xy - \beta z,\end{aligned}\tag{17}$$

and parameters $\sigma = 10, \rho = 8/3, \beta = 28$. Consolidating all the states (x, y, z) into S , the neural network tries to learn the state at the subsequent time-step (S_{t+1}) given the current state (S_t). The architecture has a single hidden layer with 100 neurons, a constant learning rate of 0.01, a hyperbolic tangent activation function (tanh), and uses parameters $\beta_1 = 0.9$ and $\beta_2 = 0.95$.

The complete dataset consists of 10000 points created using [25]. The first set of results in Figure 1 compare the traditional time stepping methods such as Forward Euler, Heun’s Method, Stability Preserving Third Order Runge Kutta (SSPRK3) and Fourth Order Runge Kutta (RK4). The x -axis in the plots represent total number of gradient evaluations, and the y -axis denotes the value of cost function. Figure 1a shows a non-stochastic training process without batching. Figure 1b and fig. 1c denotes training in batches of data while fig. 1d is the “butterfly” shape of the state trajectory. These plot shows the preliminary results with subsequent higher order Runge-Kutta methods. We continue the experiments in Figure 2, which compares the new IMEX methods. Figure 2 shows the power of IMEX

methods as it goes to a local minima very quickly (i.e faster training) with the trapezoidal method slightly beating out ADAM towards the end.

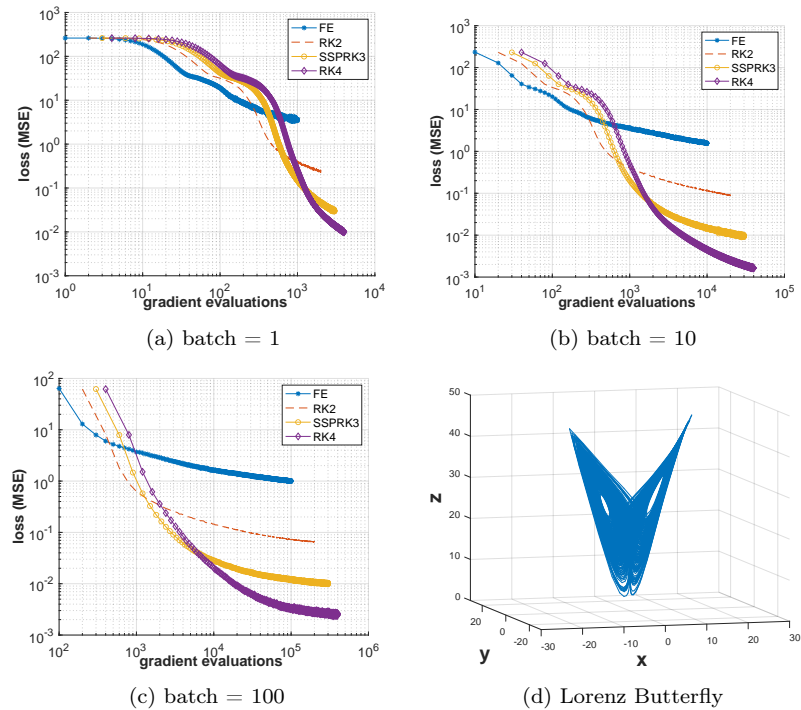


Figure 1: Regression on learning the L63 chaotic dynamics. The learning rate = 0.01, epochs = 1000, $\beta_1 = 0.9$, $\beta_2 = 0.95$ in the training process. First order Forward Euler along with subsequent higher order RK methods are compared. RK4 (4^{th} order Runge-Kutta) seems to outperform all the other methods for comparable number of gradient evaluation for both batched and mini batched training.

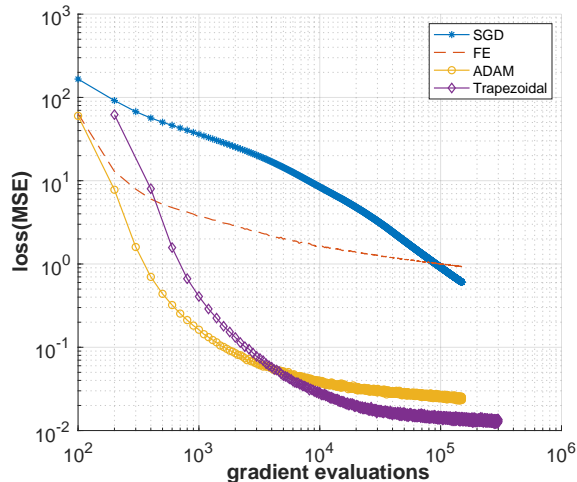


Figure 2: Regression on learning the L63 chaotic dynamics. The learning rate = 0.01, batches = 100, epochs = 1500, $\beta_1 = 0.9$, $\beta_2 = 0.95$ in the training process. SGD, Forward Euler, IMEX ADAM and IMEX Trapezoidal discretization of eq. (3) are compared. Imex Trapezoidal seems to outperform the original ADAM as learning proceeds for comparable number of gradient evaluation.

4.2 Sum of Gaussians

This is a nonlinear regression problem where the dataset is taken from National Institute of Standards and Technology (NIST) database (developed by Rust) which is a relatively hard problem to regress (atleast in our experience). We fix the parameter values at $b_1 = 94.9$, $b_2 = 0.009$, $b_3 = 90.1$, $b_4 = 113$, $b_5 = 20$, $b_6 = 73.8$, $b_7 = 140$, $b_8 = 20$ whereas the equation is:

$$f(x) = b_1 e^{-b_2 x} + b_3 e^{-\frac{(x-b_4)^2}{(b_5)^2}} + b_6 e^{-\frac{(x-b_7)^2}{(b_8)^2}}, \quad (18)$$

$$x \in [0, 250]$$

A shallow and a (relatively) deeper feedforward network is used in this experiments. Initial experiments (fig. 3) shows some promise in using traditional higher order Runge-Kutta methods. Motivated by this, we try the new IMEX methods (fig. 4).

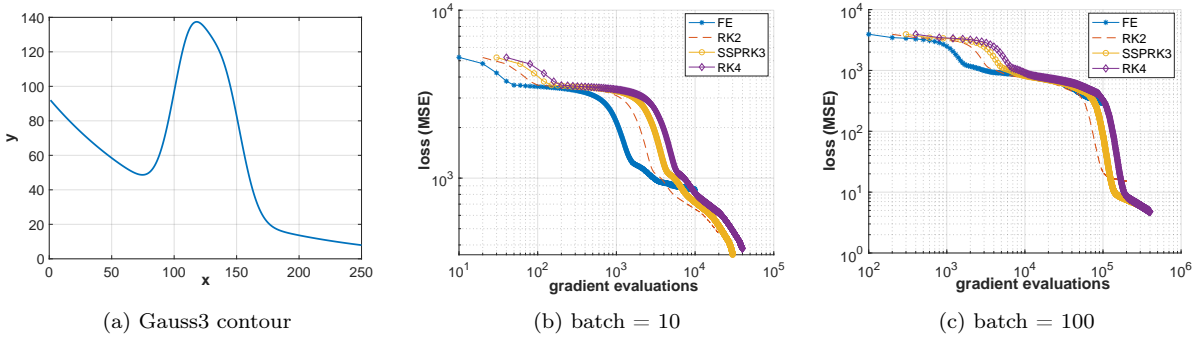


Figure 3: Non-Linear Regression on the NIST Gauss3 dataset with a shallow network and varying stochastic noise. Learning rate = 0.001, $\beta_1 = 0.9$, $\beta_2 = 0.9$, epochs = 1000 with 1 hidden layer (100 neurons). Figure 3a shows the contour of the problem in the domain $0 \leq x \leq 250$, fig. 3b denotes the learning curve with 10 batches of data while fig. 3c represents a highly stochastic training process. It seems that the higher RK methods have an advantage over lower order methods for this problem setup.

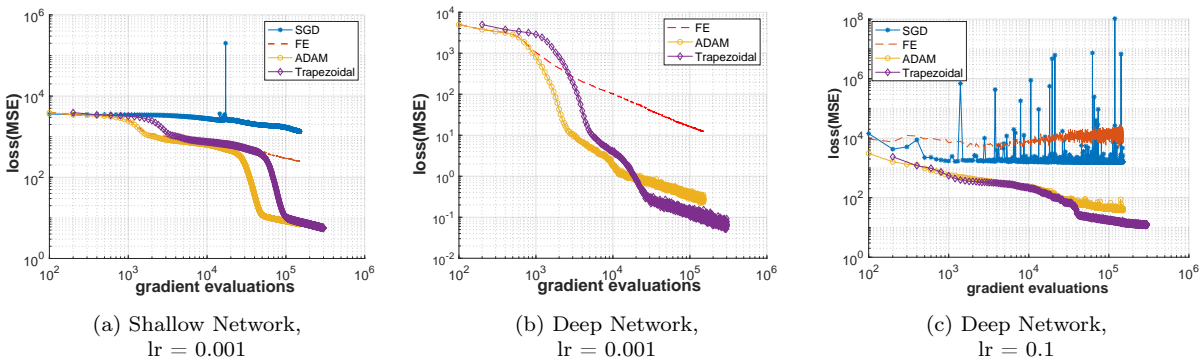


Figure 4: Non-Linear Regression on the NIST Gauss3 dataset with varying learning rates. Epoch = 1500, batch = 100, $\beta_1 = 0.9$, $\beta_2 = 0.9$, $\epsilon = 10^{-8}$. A shallow network (1 hidden layer with 100 neurons) with a stable learning rate (0.001) is depicted in fig. 4a. A (relatively) deeper network (5 hidden layers with 10 neurons in each) with a stable learning rate = 0.001 is shown in fig. 4b. Finally, a deep network with unstable learning rate = 0.1 is done to check the advantage of higher IMEX method over traditional SGD or RK methods.

Gaussian Error Linear Units (GeLU) is the activation function used with 1000 epochs. The higher order methods seem to work better in the highly stochastic training case which is interesting (refer fig. 3c). The results for the second set of plots (fig. 4) are very encouraging too. Initially a shallow network with just one hidden layer with 100 neurons is used. The experiment is run for 1500 epochs. All other hyperparameters are evident from the plots. β_2 is kept low as keeping the past squared gradient information is detrimental for this problem. The model is trained with 10000 datasets divided into 100 batches. Looking at Fig. 4a, the SGD seem to not work at all and both ADAM and Trapezoidal method are performing

better but very similar on this architecture. The decrease in loss function is not significant either. The next experiment is with a deep network with 5 hidden layers with 10 neurons in each and all other parameters and hyper-parameters are kept the same (fig. 4b). SGD completely fails in this architecture (not plotted because of scaling issues) and Trapezoidal method performs similar in the beginning but has a slightly better performance as training progresses. Looking at the results, the learning rate for this deep architecture was increased to 0.1 which is very high (and unstable) for such a deep network. SGD is unstable under such high learning rate and oscillates which is expected. Both the IMEX methods are fairly stable under such high unstable learning rate.

4.3 Spiral Dataset

The spiral (Swiss roll) dataset is a classification problem where the classifier tries to separate/classify data points from two spirals (refer fig. 5a). It is inherently difficult to train on because of high non-linearity that exists in the problem. In the experiments with traditional numerical methods, we see a promising advantage of higher order methods. Instead of a constant decrease or a schedule of learning rate, a cyclical variant often helps in reducing the number of epochs [30] and is used here. For the IMEX cases, a deeper network with 8 hidden layers with a width of 8 neurons in each is used along with a cyclic learning rate [30] which is shown in fig. 5b and SiLU activation function. There are 1000 data points divided into 10 batches. The training is carried out for 1000 epochs and the results are visualized in Figure 6.

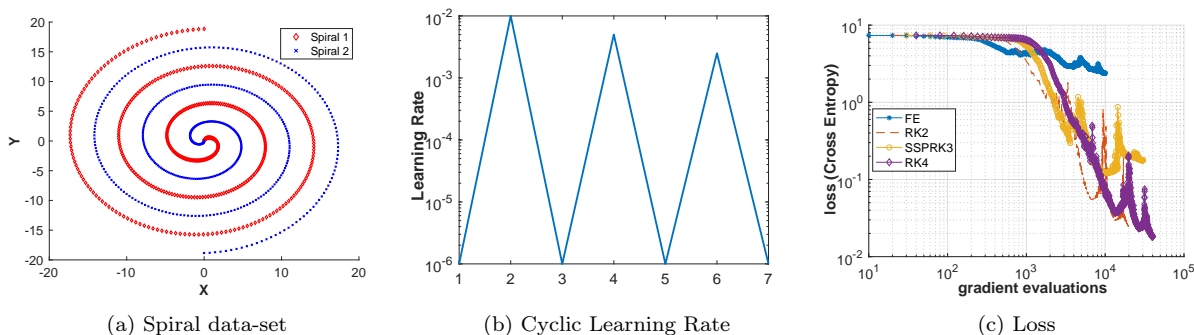


Figure 5: Binary classification on the spiral data-set with a (relatively) deeper network. Learning rate = cyclic , $\beta_1 = 0.9$, $\beta_2 = 0.999$, batch = 10 and 8 hidden layer (8 neurons). The dataset and the cyclic learning rate are visualized in fig. 5a and fig. 5b respectively while the learning curve is shown in fig. 5c. The learning curve shows some advantage of higher order RK method compared to first order RK method.

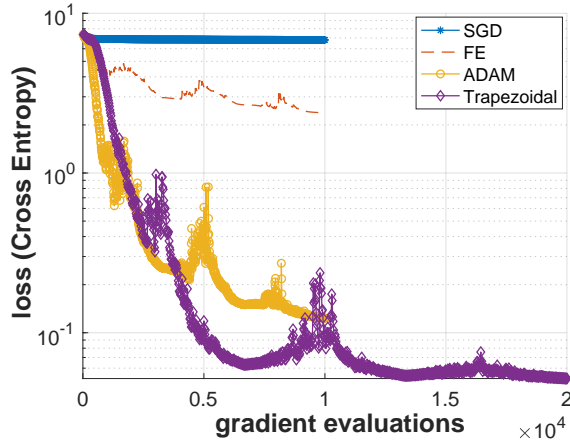


Figure 6: Binary classification on the spiral data-set with a (relatively) deeper network (8 hidden layers with 8 neurons in each). Learning rate = cyclic, epochs = 1000, batch = 10, $\beta_1 = 0.9, \beta_2 = 0.999, \epsilon = 10^{-8}$. IMEX methods seems to have some advantage over the traditional SGD or RK methods where second order Trapezoidal beats the first order ADAM slightly as the training progresses.

4.4 MNIST

MNIST is a standard benchmark dataset used for evaluating classification algorithms. MNIST consists of 60000 training data along with 10000 test data of handwritten digits. However, we reduced the training and testing set to 6000 and 1000 respectively for faster training with 500 epochs. The architecture has 2 hidden layers with 256 and 64 neurons respectively. The results can be referred to in Figure 7. The new Trapezoidal method performs slightly worse than ADAM but way better than SGD (fig. 7a). However, it is interesting to note that the adaptive methods do well in cases when learning rate are large or the hyperparameters are not the "best" with Trapezoidal method showing some advantages (fig. 7c). The accuracies for the ADAM and Trapezoidal methods are 94.7% and 94.7% respectively, for Figure 7a, 94.27% and 94.45% for Figure 7b, 94.56% and 94.43% for Figure 7c.

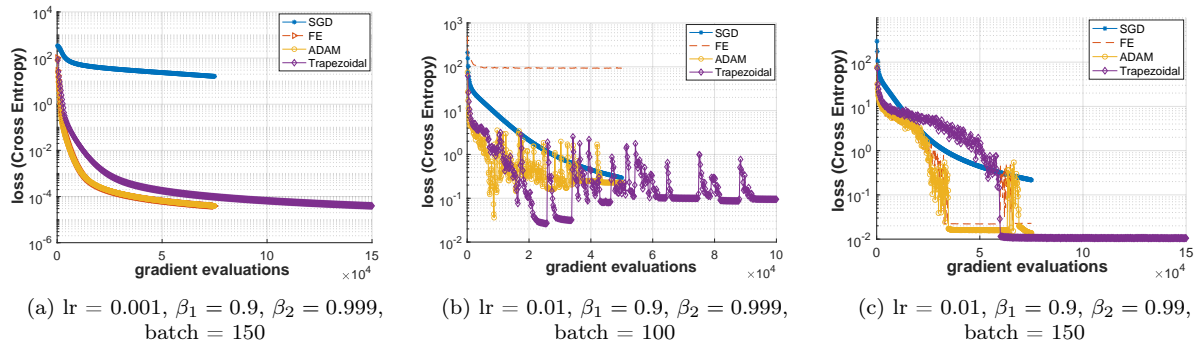


Figure 7: Classification on MNIST Dataset of Handwritten digits. The hyper-parameters are evident from the plots. Figure 7a denotes a stable learning process (due to “best”) hyperparamters and we see IMEX methods are better than standard SGD. However, second order method performs very similar to original first order IMEX ADAM and we see no advantage of a higher order method in this setup.

4.5 CIFAR10 with VGG

Convolutional Neural Networks (CNNs) are ubiquitous in image classification tasks. VGG-16 [29] is considered to be a very deep CNN which won the prize in the ImageNet Challenge 2014. We try the new IMEX methods on the CIFAR10 dataset using this architecture. The new IMEX Trapezoidal doesn’t seem to give any advantage in training for the same number of gradient evaluations. They have similar accuracies on the test data (refer fig. 8b).

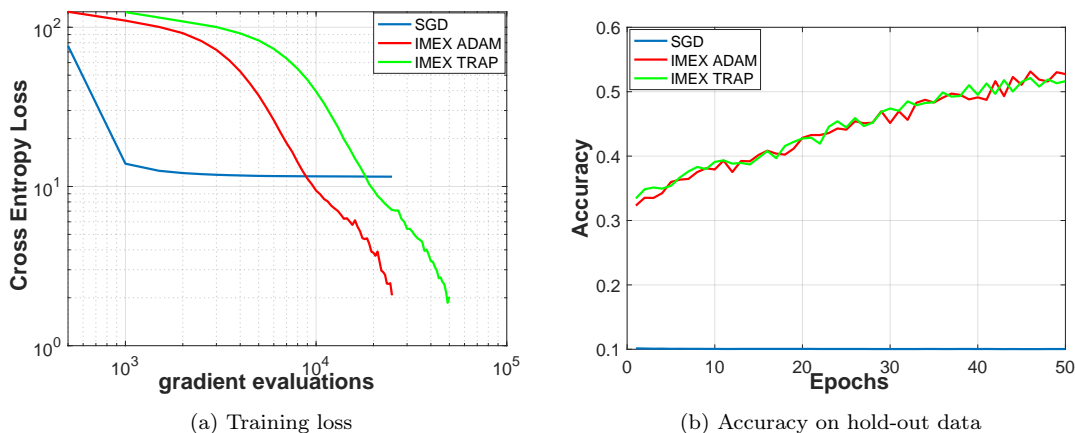


Figure 8: Classification task on the Cifar10 data using VGG architecture($lr = 0.001, \beta_1 = 0.9, \beta_2 = 0.999,$ batches = 100). The scaled training loss doesn’t seem to give us any advantage using the new trapezoidal method. The accuracy is similar (refer 8b). Both the IMEX methods are better than SGD. SGD might work with momentum or regularization techniques like dropout, ridge or lasso regression.

5 CONCLUSIONS

This work extends the stochastic optimization method ADAM [16], widely used for neural network training, to an entire family of algorithms. The starting point of the analysis is the underlying ADAM ODE eq. (3), to which the discrete ADAM algorithm converges in the limit of infinitesimally small learning rates.

We establish that the standard ADAM algorithm is the IMEX Euler discretization of the underlying ADAM ODE eq. (3). Based on this insight, we construct the new family of optimizers by applying a variety of GARK IMEX schemes (refer eq. (15)) to solve eq. (3). Employing time stepping algorithms with orders of accuracy higher than one and good stability properties can result in optimization methods with faster convergence for neural network training.

Based on a variety of numerical experiments carried out, we select the second order IMEX Trapezoidal ADAM as the method of choice, as it strikes a good balance between performance (decrease of loss function) and cost (number of gradient evaluations) per step. The new IMEX Trapezoidal ADAM outperforms standard ADAM in the Lorenz63 experiment (section 4.1), sum of Gaussians (section 4.2) and Swiss roll classification problem (section 4.3) with deep architectures. The second order method also works better under high "unstable" learning rate where SGD fails to converge.

However, for MNIST (with a standard feedforward network) and Cifar10 (with VGG [29] architecture) data, the new method seems to have no advantage over the standard ADAM for the same number of gradient evaluations. Further study is required to evaluate the need for a higher order method in such cases. The authors believe that "standard" architectures were designed to work with SGD and other first order momentum based methods. Therefore, it is possible that use of a higher order gives no substantial advantages in such architectures for the same number of gradient evaluations.

Several directions will be followed in future research. Considering the good performance of new second order method, we will study optimization algorithms based on IMEX time discretizations of order three and higher. Looking beyond IMEX GARK schemes, Linear Multistep Methods are another class of numerical time integrators that can be applied in an IMEX fashion to partitioned ODEs. Linear Multistep Methods have a natural memory built in as they keep past information (either gradients or the parameter values), and their performance will be measured against that of momentum methods [22, 32].

References

- [1] Uri M. Ascher and Linda R. Petzold. *Computer Methods for Ordinary Differential Equations and Differential-Algebraic Equations*. Society for Industrial and Applied Mathematics, USA, 1st edition, 1998.
- [2] Uri M. Ascher, Steven J. Ruuth, and Raymond J. Spiteri. Implicit-explicit runge-kutta methods for time-dependent partial differential equations. *Applied Numerical Mathematics*, 25(2):151–167, 1997. Special Issue on Time Integration.
- [3] Yoshua Bengio. *Practical Recommendations for Gradient-Based Training of Deep Architectures*, pages 437–478. Springer Berlin Heidelberg, Berlin, Heidelberg, 2012.
- [4] Tom B. Brown, Benjamin Mann, Nick Ryder, Melanie Subbiah, Jared Kaplan, Prafulla Dhariwal, Arvind Neelakantan, Pranav Shyam, Girish Sastry, Amanda Askell, Sandhini Agarwal, Ariel Herbert-Voss, Gretchen Krueger, Tom Henighan, Rewon Child, Aditya Ramesh, Daniel M. Ziegler, Jeffrey Wu, Clemens Winter, Christopher Hesse, Mark Chen, Eric Sigler, Mateusz Litwin, Scott Gray, Benjamin Chess, Jack Clark, Christopher Berner, Sam McCandlish, Alec Radford, Ilya Sutskever, and Dario Amodei. Language models are few-shot learners, 2020.
- [5] J.C. Butcher. Numerical methods for ordinary differential equations in the 20th century. *Journal of Computational and Applied Mathematics*, 125(1):1–29, 2000. Numerical Analysis 2000. Vol. VI: Ordinary Differential Equations and Integral Equations.
- [6] Augustin Cauchy et al. General method for solving systems of equations simultaneously. *Comp. Rend. Sci. Paris*, 25(1847):536–538, 1847.
- [7] Dami Choi, Christopher J. Shallue, Zachary Nado, Jaehoon Lee, Chris J. Maddison, and George E. Dahl. On empirical comparisons of optimizers for deep learning. *CoRR*, abs/1910.05446, 2019.
- [8] C. F. Curtiss and J. O. Hirschfelder. Integration of stiff equations*. *Proceedings of the National Academy of Sciences*, 38(3):235–243, 1952.
- [9] André Belotto da Silva and Maxime Gazeau. A general system of differential equations to model first order adaptive algorithms, 2019.
- [10] John Duchi, Elad Hazan, and Yoram Singer. Adaptive subgradient methods for online learning and stochastic optimization. *Journal of Machine Learning Research*, 12(61):2121–2159, 2011.
- [11] Xavier Glorot and Yoshua Bengio. Understanding the difficulty of training deep feedforward neural networks. In Yee Whye Teh and Mike Titterton, editors, *Proceedings of the Thirteenth International Conference on Artificial Intelligence and Statistics*, volume 9 of *Proceedings of Machine Learning Research*, pages 249–256, Chia Laguna Resort, Sardinia, Italy, 13–15 May 2010. PMLR.

- [12] E. Hairer, S.P. Nørsett, and G. Wanner. *Solving Ordinary Differential Equations I Nonstiff problems*. Springer, Berlin, second edition, 2000.
- [13] Ernst Hairer and Gerhard Wanner. *Solving Ordinary Differential Equations II. Stiff and Differential-Algebraic Problems*, volume 14. Springer, 01 1996.
- [14] Kaiming He, Xiangyu Zhang, Shaoqing Ren, and Jian Sun. Deep residual learning for image recognition. In *Proceedings of the IEEE Conference on Computer Vision and Pattern Recognition (CVPR)*, June 2016.
- [15] Christopher A. Kennedy and Mark H. Carpenter. Additive runge–kutta schemes for convection–diffusion–reaction equations. *Applied Numerical Mathematics*, 44(1):139–181, 2003.
- [16] Diederik P. Kingma and Jimmy Ba. Adam: A method for stochastic optimization, 2017.
- [17] Diederik P Kingma and Max Welling. Auto-encoding variational bayes, 2013.
- [18] Robert Kleinberg, Yuanzhi Li, and Yang Yuan. An alternative view: When does sgd escape local minima?, 2018.
- [19] Alex Krizhevsky, Ilya Sutskever, and Geoffrey E Hinton. Imagenet classification with deep convolutional neural networks. *Communications of the ACM*, 60(6):84–90, 2017.
- [20] Edward N. Lorenz. Deterministic nonperiodic flow. *Journal of Atmospheric Sciences*, 20(2):130 – 141, 1963.
- [21] Meenal V. Narkhede, Prashant P. Bartakke, and Mukul S. Sutaone. A review on weight initialization strategies for neural networks. *Artif. Intell. Rev.*, 55(1):291–322, jan 2022.
- [22] Yurii Nesterov. A method for unconstrained convex minimization problem with the rate of convergence $o(1/k^2)$. *Proceedings of the USSR Academy of Sciences*, 269:543–547, 1983.
- [23] Boris Polyak. Some methods of speeding up the convergence of iteration methods. *Ussr Computational Mathematics and Mathematical Physics*, 4:1–17, 12 1964.
- [24] Sashank J. Reddi, Satyen Kale, and Sanjiv Kumar. On the convergence of adam and beyond, 2019.
- [25] Steven Roberts, Andrey A Popov, Arash Sarshar, Reid Gomillion, and Adrian Sandu. *Computationalscielaboratory/ode-test-problems: v0.0.1*, June 2022.
- [26] Adrian Sandu and Michael Günther. A generalized-structure approach to additive Runge–Kutta methods. *SIAM Journal on Numerical Analysis*, 53(1):17–42, 2015.
- [27] Chi-Wang Shu. Total-variation-diminishing time discretizations. *SIAM Journal on Scientific and Statistical Computing*, 9(6):1073–1084, 1988.

- [28] Chi-Wang Shu and Stanley Osher. Efficient Implementation of Essentially Non-oscillatory Shock-Capturing Schemes. *Journal of Computational Physics*, 77(2):439–471, August 1988.
- [29] Karen Simonyan and Andrew Zisserman. Very deep convolutional networks for large-scale image recognition, 2015.
- [30] Leslie N. Smith. Cyclical learning rates for training neural networks. In *2017 IEEE Winter Conference on Applications of Computer Vision (WACV)*, pages 464–472, 2017.
- [31] Nitish Srivastava, Geoffrey Hinton, Alex Krizhevsky, Ilya Sutskever, and Ruslan Salakhutdinov. Dropout: A simple way to prevent neural networks from overfitting. *Journal of Machine Learning Research*, 15(56):1929–1958, 2014.
- [32] Weijie Su, Stephen Boyd, and Emmanuel J. Candes. A differential equation for modeling nesterov’s accelerated gradient method: Theory and insights, 2015.
- [33] Ilya Sutskever, James Martens, George Dahl, and Geoffrey Hinton. On the importance of initialization and momentum in deep learning. In Sanjoy Dasgupta and David McAllester, editors, *Proceedings of the 30th International Conference on Machine Learning*, volume 28 of *Proceedings of Machine Learning Research*, pages 1139–1147, Atlanta, Georgia, USA, 17–19 Jun 2013. PMLR.
- [34] Tijmen Tieleman, Geoffrey Hinton, et al. Lecture 6.5-rmsprop: Divide the gradient by a running average of its recent magnitude. *COURSERA: Neural networks for machine learning*, 4(2):26–31, 2012.
- [35] Manzil Zaheer, Sashank Reddi, Devendra Sachan, Satyen Kale, and Sanjiv Kumar. Adaptive methods for nonconvex optimization. In S. Bengio, H. Wallach, H. Larochelle, K. Grauman, N. Cesa-Bianchi, and R. Garnett, editors, *Advances in Neural Information Processing Systems*, volume 31. Curran Associates, Inc., 2018.
- [36] Matthew D. Zeiler. Adadelta: An adaptive learning rate method, 2012.

APPENDIX

A ADAM

The original ADAM is listed below where θ s are the learnable parameters, m is the momentum that captures the past gradients and v is the velocity which captures the square of the past gradients [16]. The original literature has bias correction term to correct for the zero initialization of exponential moving average. That correction is not included here.

Algorithm 2 The ADAM algorithm for solving stochastic optimization problems. Some default values are $h = 0.001$, $\beta_1 = 0.9$, $\beta_2 = 0.999$, $\epsilon = 10^{-8}$

Require: h : Stepsize

Require: $\beta_1, \beta_2 \in [0, 1)$: Exponential decay rates for the momentum estimates.

Require: $\mathcal{L}(\theta)$: Loss/Objective function to be minimized

Require: θ_0 : Initial values of the weights/biases

$m_0 \leftarrow 0$ // Initialize first moment vector
 $v_0 \leftarrow 0$ // Initialize second moment vector
 $n \leftarrow 0$ // Initialize time/iteration no.

while θ_n not converged **do**

 // Calculate gradient at time $n + 1$

$g_{n+1} \leftarrow \nabla_{\theta} \mathcal{L}(t_{n+1}; \theta_n)$

 // Update momentum and velocity

$m_{n+1} \leftarrow \beta_1 \circ m_n + (1 - \beta_1) \circ g_{n+1}$

$v_{n+1} \leftarrow \beta_2 \circ v_n + (1 - \beta_2) \circ g_{n+1}^2$

$\theta_{n+1} \leftarrow \theta_n - h \circ m_{n+1} / (\sqrt{v_{n+1}} + \epsilon)$

$n \leftarrow n + 1$

end while

B Higher Order IMEX Methods

This section introduces 2 more higher order methods that are developed for the underlying ODE in Section 3 and the satisfying the order conditions in [26]. As mentioned earlier, a time integration method can be characterized entirely by it's Butcher tableaus and we proceed to provide the parameterized tableaus for the methods.

	0	0	0	0	0	0	0
Explicit	1	1	0	0	1	0	0
$\frac{1}{2}$	$\frac{1}{4}$	$\frac{1}{4}$	0	0	0	$\frac{1}{2}$	0
	0	0	0	0	$\frac{1}{6}$	$-\frac{1}{3}$	$\frac{1}{6}$
Implicit	$\frac{1}{2}$	$\frac{1}{2} - l_{22}$	l_{22}	0	$\frac{1}{6}$	$\frac{5}{12}$	$-\frac{1}{12}$
	1	$-1 + 8l_{22} + l_{32}$	l_{32}	$2 - 8l_{22} - 2l_{32}$	$\frac{1}{6}$	$\frac{2}{3}$	$\frac{1}{6}$
	$\frac{1}{6}$	$\frac{1}{6}$	$\frac{2}{3}$		$\frac{1}{6}$	$\frac{2}{3}$	$\frac{1}{6}$

(19)

The tableau (eq. (19)) incorporates a third order SSP method [27, 28] for updating the explicit part of the underlying IMEX formulation and a LobattoIIIC methods for updating the implicit part [12, 13]. The coupling coefficients are derived from satisfying underlying order conditions. LobattoIIIC are both L-stable and has algebraic stability. l_{22} and l_{32} are parameters that can be tuned to get different methods. This method will be called "*SSPRK3LOBATTOIIC*" in the experiment.

	0	0	0	0	0	0	0	0	0
Explicit	$\frac{1}{2}$	$\frac{1}{2}$	0	0	$\frac{1}{2}$	0	0	0	0
	$\frac{1}{2}$	0	$\frac{1}{2}$	0	0	$\frac{1}{2}$	0	0	0
	1	0	0	1	0	0	1	0	0
	0	0	0	0	$\frac{1}{6}$	$-\frac{1}{3}$	$\frac{1}{6}$		
Implicit	$\frac{1}{2}$	$\frac{1}{4}$	$\frac{1}{4}$	0	$\frac{1}{6}$	$\frac{5}{12}$	$-\frac{1}{12}$		
	1	0	α	$1 - \alpha$	$\frac{1}{6}$	$\frac{2}{3}$	$\frac{1}{6}$		
	$\frac{1}{6}$	$\frac{1}{3}$	$\frac{1}{3}$	$\frac{1}{6}$	$\frac{1}{6}$	$\frac{2}{3}$	$\frac{1}{6}$		

(20)

The tableau (eq. (20)) applies a RK4 method for the explicit part and a LobattoIIIC for the implicit part. The coupling coefficients are derived from satisfying the order conditions. It is to be noted that there are several new methods that can be explored through the IMEX formulation. We enlisted just two that were tried out. α is the parameter that can be tuned. This method will be called "*RK4LOBATTOIIC*" in the experiment.

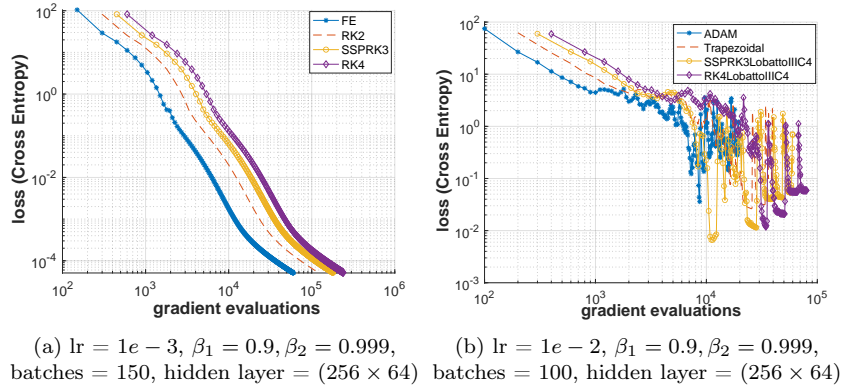


Figure 9: Classification on the MNIST dataset

A single experiment has been reported here using the newer higher order methods compared to IMEX Euler and IMEX Trapezoidal methods (fig. 9b). The corresponding parameters are $l_{22} = 0.2, l_{32} = 0.1$ and $\alpha = 0.5$. The user is free to tune these parameters as deemed fit. One may look at the stability plot for these methods too (although there is no concrete proof that it will always work well!). The batches are made lower with a higher learning rate to check the performance of the newer methods under unstable/unfavorable

hyperparameters. The newer higher order methods goes to a lower minima compared to the initial 2 methods. However, they are oscillatory due to higher learning rate leading to it getting stuck in a local minima. Parameter tuning (l_{22}, l_{32}, α) for the new higher order methods might work better and needs further investigation.